IEEE Access
Multidisciplinary | Rapid Review | Open Access Journal

Received July 24, 2020, accepted August 3, 2020, date of publication August 6, 2020, date of current version August 20, 2020.

Digital Object Identifier 10.1109/ACCESS.2020.3014832

LIDAR-Assisted Wind Turbine Structural Load Reduction by Linear Single Model Predictive Control

RAFAEL BARCENA[1], (Member, IEEE), TATIANA ACOSTA[2], AINHOA ETXEBARRIA[1], AND INIGO KORTABARRIA[1], (Member, IEEE)

[1]Electronics Technology Department, Faculty of Engineering in Bilbao, University of the Basque Country (UPV/EHU), 48013 Bilbao, Spain
[2]Departamento de Eléctrica y Electrónica, Universidad de la Fuerzas Armadas—ESPE, Sangolquí 1715231, Ecuador

Corresponding author: Rafael Barcena (rafa.barcena@ehu.es)

This work was supported in part by the Universidad de las Fuerzas Armadas ESPE and the University of the Basque Country UPV/EHU.

ABSTRACT *LIght Detection And Ranging* (LIDAR) sensors provide preview measurements of wind speed in front of the device. This preview may be used to improve important aspects of the operation of wind turbines, such as structural load, while limiting the control effort. In this paper, a single model-based predictive controller, taking advantage of the incoming wind in advance LIDAR measurements, is applied to the generator torque reference of the wind turbine in order to reduce torsional shaft vibrations. The controlled system is tested in a simulation environment that reproduces a set of gusts and turbulent wind fields above the nominal, where the structural loads are higher. The performances obtained are compared with the baseline and with those extracted from a single model predictive controller version without disturbance previsualization. Then, the effect of the coherence between the effective wind estimated from the LIDAR measurements and the real wind is considered. The practical implementation is demonstrated on real-time controller prototypes applied to a Hardware-In-the-Loop Simulator that reproduces realistically the dynamic behavior of the *National Renewable Energy Laboratory* 5 MW reference wind turbine.

INDEX TERMS LIDAR, disturbance preview, feedforward control, model-based predictive control, hardware-in-the-loop simulation, load reduction, practical implementation, parameter uncertainty, real-time control, wind turbine.

I. INTRODUCTION

One of the main objectives of wind turbines (WT) control is to reduce fatigue and extreme loads on the drive train and blades, while keeping the control action limited and the generated power stable. Improvements in these aspects result in a longer lifetime for the turbine, as well as a reduction in maintenance, thus lowering the cost of energy. However, this is a difficult task, as the transients caused by the bursts and turbulence represent unknown disturbances to the controller. Feedback-based controllers can only compensate for such transients with a delay, when their effects are shown at the system outputs and the WT actuators propagate the corresponding generated control action. Such a delay could be compensated for by using a controller that includes feedforward action, but a sufficiently early preview measurement of such disturbances is required. A Doppler LIDAR may provide such a measurement.

The feedforward control to manage WT is first proposed in [1] , using measurements from a weather tower, as LIDAR sensors were then still too expensive. Later, the use of optical fiber substantially reduced the costs, and LIDAR started to be used for remote measurements of incoming wind [2]. Since then, LIDAR-based turbine control has been studied for both below (region 2) and above (region 3) nominal winds. However, it was demonstrated -see [3] and [4]- that the improvements obtained in the energy capture did not compensate sufficiently the disadvantages associated with the LIDAR-assisted control (structural load and torque fluctuations) for WT in region 2. Therefore, much work has been focused on using LIDAR-assisted preview-based control to regulate the rotor speed and mitigate the structural loads in

The associate editor coordinating the review of this manuscript and approving it for publication was Ahmed F. Zobaa.

region 3. In fact, the potential of this approach has been extensively demonstrated by using both the effective wind preview throughout the rotor for collective pitch control, [5]–[14], and on each blade for individual pitch control, [15]–[17]. In addition, the LIDAR-assisted control of the yaw or speed has also been studied to improve the extracted energy, [18], [19]. Comprehensive reviews of the related literature as well as critical discussions on the state of the art and future of the LIDAR-assisted wind turbine control may be found in [20]–[22].

The mentioned controllers range from simple feedforwards, based on inverse models -see e.g. [9]-, to more complex model predictive controllers (MPC). These MPCs use the previsualization of the disturbance caused by the incoming wind in order to optimize the control actions during the prediction horizon, avoiding to some extent the effects of the estimation delay, appeared in the controllers based on feedback [10], [14], [15], which causes a substantial improvement in the performance of the controlled system. However, it soon became clear that the improvement achieved in this way is largely conditioned by the quality of the effective wind measurement that can be taken in practice by the installed LIDAR. On the other hand, the LIDAR-assisted MPC faces the same practical implementation problems as the MPC without preview. The handling of highly non-linear wind turbine dynamics means that a trade-off between performance and computational load must always be made. Moreover, it is very difficult to ensure in advance the formal stability of such controllers and, even more, without drastically limiting their performance. A solution to these implementation problems is based on using a single linear model of the wind turbine in the internal prediction of the MPC, for the whole range of wind speeds in the region 3 -see reference [23] for further details-.

This work describes a Single Model Predictive Control (SMPC) controller that uses the same single linear turbine model and settings already presented in [23], but now also incorporating the prediction of the disturbance posed by fluctuations in the aerodynamic torque, caused by alterations in the incoming effective wind, realistically measured by a LIDAR system. The control goal again focuses on the reduction of the structural load on the transmission train, without excessively altering the generated power. The performance achieved by this controller is compared with the baseline and with one of those presented in [23]. Finally, such comparison is related to the quality of the available preview effective wind measurement.

The paper is organized as follows: Section II presents how the incoming disturbance is extracted from the measurements obtained in advance by the LIDAR and explains how it fits into the SMPC approach, described in [23] for the case when no disturbance previsualization is available. Then, Section III summarizes the comparative results obtained from a perfect disturbance previsualization in order to study the potential performance of the proposal. To do so, the *National Renewable Energy Laboratory* (NREL) 5 MW reference turbine is exposed to coherent gusts and three-dimensional stochastic wind fields. Such a study is carried out based on both numerical simulations and using real-time controller prototypes, applied to the *Hardware-in-the-Loop* (HiL) wind turbine simulator, also used in [23] but conveniently modified. In section IV, the obtaining of realistic LIDAR measurements is described, and, in Section V, the reduction on the structural load, obtained as a function of the quality of the LIDAR preview, is presented and commented. Finally, Section VI concludes the paper with a summary and the future perspectives of the work.

II. LIDAR-ASSISTED LINEAR SMPC

The SMPC controllers presented in [23] use a single internal linear model to obtain the behavior of the WT rotor and drive-train during the prediction horizon. Such a model is a three-mass model, for the mechanical part, in series with the dynamic model of the generator electric behavior. The mechanical model considers the inertia of the effective flexible part of the blades J_{bl}, the inertia of the rigid part of the blades plus the hub J_{hub} and the inertia of the generator J_{gen}. Such three masses are linked by two flexible elements representing the stiffness and damping of the blades and drive-train. The inputs to the internal model are, at one end, the aerodynamic torque T_{aero} that the incident wind applies on the blades and, at the other, the generator torque reference T^*_{em} provided by the controller. T_{aero} is considered a measured disturbance (MD) and T^*_{em} is the manipulated variable (MV). When no measurements of the effective wind W_m on the rotor are available, the aerodynamic torque T_{aero} must be estimated from its effects on the angular speed of the generator ω_{gen}. This may be done either by external preprocessing or by taking advantage of the MPC state observer -see section III. D. in [23] for details-. In both cases, the estimation suffers from a certain delay that impairs the performance achieved in reducing the structural load.

Now, we assume that the incoming wind measurements obtained through a LIDAR focused at a certain distance from the rotor are used to calculate the effective wind W_m that will affect the WT, with some anticipation. This anticipation depends namely on the focal distance and the average speed of the wind, and the assumption is made that it will be greater than the duration of our SMPC prediction horizon. Obviously, it will be also necessary to estimate the aerodynamic torque T_{aero} that such effective wind W_m will induce in our rotor of radius R. In order to do so, the reduced aerodynamic model, already presented in [23], is utilized:

$$T_{aero} = \frac{1}{2}\rho\pi R^3 \frac{C_P(\lambda,\beta)}{\lambda} W_m^2 = 0.5\rho\pi R^2 W_m^3 \frac{C_P(\lambda,\beta)}{\omega_{rot}}$$
$$being:\ \lambda = \frac{\omega_{rot} R}{W_m} \tag{1}$$

where ρ is the air density, β the pitch angle, λ is the tip speed ratio, ω_{rot} the angular speed of the rotor and C_p the effective power coefficient, implemented as a *look-up* table and extracted from steady-state simulations of the NREL 5MW turbine with *WT_Perf* [24].

The processing of the model (1) that allows implementing the T_{aero} preview starts with the accumulation in buffers of enough input data to fulfill its evolution during the prediction horizon (N samples). It is clear that we do not have future values for the pitch angle β and rotor speed ω_{rot}, since they depend on the action of the pitch control loop that is not included in the model. However, the dynamic behavior of that loop and, therefore, of those variables, is much slower than the control of the torque of the generator we are dealing with. This allows us to update, at each sampling time, the complete content of such buffers with the N-times repeated current measurement of such variables.

As can be seen in Figure 1, the model (1) is computed to obtain, at each sampling instant, the preview of T_{aero}, defined as a measured disturbance (MD) in the SMPC. Later, this preview is introduced in the internal model, giving rise to an approach similar to the version 1 of the SMPC controller described in section III. D. 1. of [23]. In that case, as no disturbance preview was available, the disturbance was considered equal to the last calculated value over the whole prediction horizon. Since this calculation is always obtained with a certain delay, the control action cannot anticipate the arrival of important changes in the incident wind. However, by having a preview of the disturbance, the controller may predict the effect on the system in time to compensate for the control action delays (algorithm execution, instrumentation, actuator,...), improving in many cases the resulted performance, without the need to increase the control action.

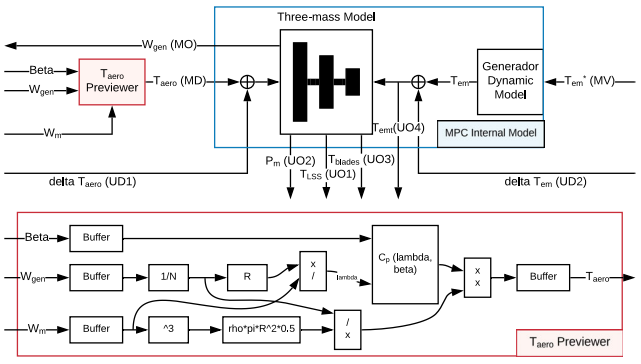

FIGURE 1. Internal model and disturbance estimator for the SMPC LIDAR-assisted version.

As in that case, the internal model is also provided with an additional input ΔT_{aero}–see figure 1-, defined as an unmeasured disturbance (UD1), in order to give robustness to the approach, given the errors prone to occur in the T_{aero} previewer. These errors can take place due to multiple causes, namely, the aerodynamic model of the turbine, the measurement of the effective wind W_m and the approximation made for the ''prediction'' values for β and ω_{rot}. Assuming that such errors may turn out to be persistent, the SMPC internal model is extended with a new state –an integrator is used as an input disturbance model for ΔT_{aero}- and the *Kalman* filter, incorporated in the SMPC controller, is in charge of estimating its value. The same procedure may be used to estimate the entire input unmeasured disturbance, not only the errors made in its calculation, and obtain good control results. In fact, the alternative controller version SMPC UD, which is used for comparison in this study, works in this way –see section III.D.2. of [23] for details-.

Note 1: Observe that the preview calculation described above requires the use of a nonlinear function to calculate the C_P effective power coefficient. However, this calculation is implemented outside the internal model of the MPC controller, thus allowing us to maintain the use of a single linear internal model and the advantages that this entails. Note that these advantages include a low computational burden and, most importantly, the *in advance* proof of stability based on the application of a terminal weight on the system states. Such terminal weight is obtained easily from a simple matrix *Lyapunov* equation and does not represent a notable limitation on the performance of the controlled system –see section III. C. of [23] for details-.

III. CONTROLLER POTENTIAL PERFORMANCE

In this section, it will be assumed that the effective wind calculated from the LIDAR measurements coincides exactly with the real one. This is carried out to make the effect of disturbance previsualization more apparent and better analyze the reachable potential (maximum) performance. First, the comparative results are obtained using numerical simulations. Then, the modifications made in the HiL simulator of the NREL 5 MW WT, used in [23], are described. Such modifications allow the real-time implementation of the LIDAR-assisted version. Finally, we present the comparative results obtained in such experimental testing. In both studies, the settings that impose the aggressiveness of the controller and the speed of the state observer are the same as those used in [23].

A. SIMULATION RESULTS

For this controller with disturbance preview, the most important improvements may be expected in the reduction of extreme loads when wind gusts episodes occur. However, it can also significantly reduce fatigue loads and, therefore, both cases are investigated in this section.

1) EXTREME LOADS

As in section IV. A. in [23], hub height time series have been created with extreme operation gusts according to IEC standard [25] at $v_{rated} + 2$ m/s $= 13.2$ m/s and $v_{out} = 25$ m/s, being v_{rated} and v_{out} the rated and cut-out wind speeds for the NREL 5MW WT, respectively. Then, the performance of the LIDAR-assisted (MDL) and the compact version 2 (UD) –see section III. D. 2. in [23]- SMPC controllers are compared with the baseline in *Table* 1. Besides, in order to check the robustness to modeling errors, increments on the mass (ice, dust, ...) of the rotor has been considered. Specifically, changes on J_{bl} and J_{hub} inducing a 10 % alteration on the natural frequencies of the mechanical system have been

TABLE 1. Percentage reduction in T_{LSS} for extreme loads.

Results		Numerical Simulations				Real-Time Experiments			
Model error		0 %		10 %		0 %		10%	
MPC version		MDL	UD	MDL	UD	MDL	UD	MDL	UD
Gust $v_{rated}+2$	$MaxT_{LSS}$	-98.4	-88.4	-76.5	-96.3	-97.3	-41.7	-74.6	-52.3
	σ (T_{LSS})	-90.1	-89.7	-83.9	-97.6	-90.0	-49.3	-82.0	-60.4
Gust v_{out}	$MaxT_{LSS}$	-94.1	-85.5	-83.7	-90.2	-91.8	-45.1	-81.9	-46.4
	σ (T_{LSS})	-77.7	-77.4	-76.6	-81.2	-77.4	-43.7	-74.6	-46.8

introduced in the WT model and the related results added to such comparison.

Specifically, the maximum ($MaxT_{LSS}$) and standard (σ) deviations (% reduction with respect to baseline) on the torsional torque on the *low-speed* turbine shaft (T_{LSS}) are presented in *Table* 1. The improvement obtained by MDL control is very high with respect to the baseline case, but not much greater than that achieved by the UD controller, without preview. This is probably due to the intense adjustment of the state observer used here. Such adjustment manages to reduce to the minimum the delay in the internal estimation of the T_{aero} disturbance. Furthermore, as expected, it is also noted in *Table* 1 that the robustness to modeling errors is better in the UD controller, given that its performance does not depend so much on the internal model by having more *feedback* action.

2) FATIGUE LOADS

As in section IV. B in [23], to evaluate the fatigue load, a set of A-type turbulent wind fields according to IEC 61400-1 [25] in full-load operation region (mean wind speeds of 14, 18 and 24) generated with *Turbsim* [26] has been applied to the simulation environment. Then, the lifetime *Damage Equivalent Loads* (DEL) for the *low-speed* shaft torsion torque (T_{LSS}) were calculated on the basis of a rainflow counting with *Wohler* exponent of 4, typical for steel generator shafts [27]. The maximum (DEL), standard (σ) T_{LSS} deviations (% reduction to baseline), and power mean increase were also computed and presented in *Table 2*. The observed fatigue load reduction in slightly better in the LIDAR-assisted case, and the robustness is conserved.

TABLE 2. Percentage reduction in T_{LSS} for fatigue loads.

Results		Numerical Simulations				Real-Time Experiments			
Model error		0 %		10 %		0 %		10%	
MPC version		MDL	UD	MDL	UD	MDL	UD	MDL	UD
Wind 14 m/s 18 %	DEL T_{LSS}	-92.8	-90.5	-77.2	-85.1	-86.3	-51.9	-76.0	-47.3
	σ (T_{LSS})	-94.8	-93.2	-82.5	-90.9	-88.7	-56.2	-81.1	-57.7
	Mean POW	0.54	0.55	0.66	0.66	0.72	0.78	0.81	0.87
Wind 18 m/s 17 %	DEL T_{LSS}	-91.1	-87.8	-78.2	-87.5	-82.8	-31.6	-70.4	-34.1
	σ (T_{LSS})	-94.5	-92.7	-85.6	-93.1	-85.9	-46.9	-80.3	-52.2
	Mean POW	0.07	0.08	0.14	0.14	-0.03	0.05	-0.03	0.07
Wind 24 m/s 15 %	DEL T_{LSS}	-90.6	-88.4	-72.1	-83.7	-81.8	-33.7	-70.6	-27.0
	σ (T_{LSS})	-93.1	-91.6	-80.9	-90.1	-85.5	-41.4	-79.3	-43.7
	Mean POW	0.16	0.17	0.15	0.17	0.06	0.15	0.02	0.14

B. ADAPTED REAL-TIME EXPERIMENTAL PLATFORM

The Real-Time (RT) control experiments are implemented on the hardware platform described in [23], section V. It is composed conceptually by two elements: a WT Hardware-in-the-Loop (HiL) simulator, that reproduces the scaled behavior of the 5 MW NREL turbine on a mechanically coupled motor-generator set, and a rapid-prototyping system, devoted to put the turbine controllers into action and analyze their computational burden. The WT HiL simulator uses RT software to compute the aerodynamic and mechanical turbine models and, then, an electric motor to impose the resulting action on the generator shaft. On the other hand, the RT control platform implements the pitch, the generator, and the grid-side converter controllers. Anyway, given that the LIDAR-assisted version of the SMPC controller needs some new inputs (β and the wind preview W_m from the LIDAR), the experimental setup is correspondingly modified.

The block diagram explaining the modified platform is presented in Figure 2, where the LIDAR block is dedicated to prepare the SMPC controller effective wind previsualization W_m. By now, such a preview is identical to the delayed signal W_a, created with *Turbsim,* feeding the aerodynamic model located inside the HiL WT simulator. Evidently, such delay matches the prediction horizon used in the SMPC controller.

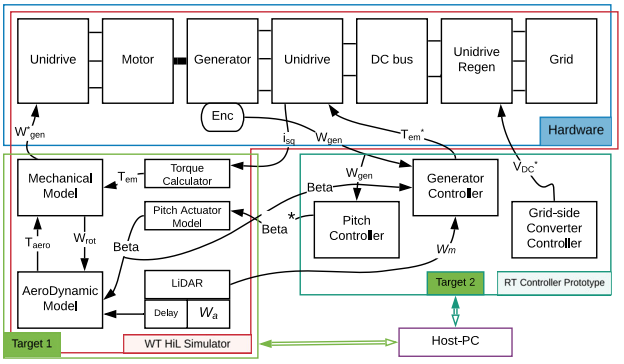

FIGURE 2. Adapted experimental platform scheme.

C. REAL-TIME CONTROL EXPERIMENTS RESULTS

The same experiments described in section III.A. have been implemented in deterministic real-time (RT) on the described experimental platform. Anyway, both control and observer setup have been relaxed –exactly as in [23]- in order to reduce the disturbances on the generated power and attain a more robust behavior for the controlled system under intense measurement noise.

1) EXTREME LOADS

The signals of interest, measured in the RT experimental platform, when applying the two SMPCs and the baseline controller under an extreme operation gust, according to IEC standard, at $v_{out} = 25$ m/s, are depicted in Fig. 3. Namely, the actual pitch angle β, the rotor angular speed ω_{rot}, the generator torque T_{em}, the torsional torque referred to the *low-speed* shaft T_{LSS} and the mechanical power ($T_{em}\omega_{gen}$) are presented.

Note 2: Note that the actual pitch β has been extracted from the RT execution of the pitch actuator model in the WT HiL simulator and then provided as a voltage input to the RT control prototype, in order to emulate a blade angular position sensor output. The ω_{rot} is derived from the measured ω_{gen}, T_{em} is obtained from the measured currents on the generator machine (i_{sq}) and the mechanical power by multiplying such measured ω_{gen} and $T_{em.}$ In this way, the RT control results incorporate the effects of the common WT instrumentation. Anyway, nowadays the wind turbines often incorporate additional sensors, e.g. in the hub for ω_{rot}, or strain gauges in the root of the blades, from which the T_{blades} torque of our internal model can be obtained -see Figure 1 and [23] for details-. Such signals may be also emulated by hardware in the context of our WT HiL simulator, as it is done for β, to provide more measured outputs to the SMPC controllers. In this way, the robustness against modeling errors could be substantially improved and the important effect of the realistic measurements better taken into account.

To facilitate a clear analysis of the disturbance previsualization effect in Fig. 3 and 4, errors in the internal model are avoided in these RT experiments and a detailed comparison of the manipulated variable T^*_{em} is presented in Fig. 4. It is evident that the control action of the MDL version -see temporal evolution of the manipulated variable T^*_{em}- anticipates the appearance of the disturbance –wind gust-, reducing the torsion of the axis with respect to the UD case, in which this preview is not available. Moreover, such an important

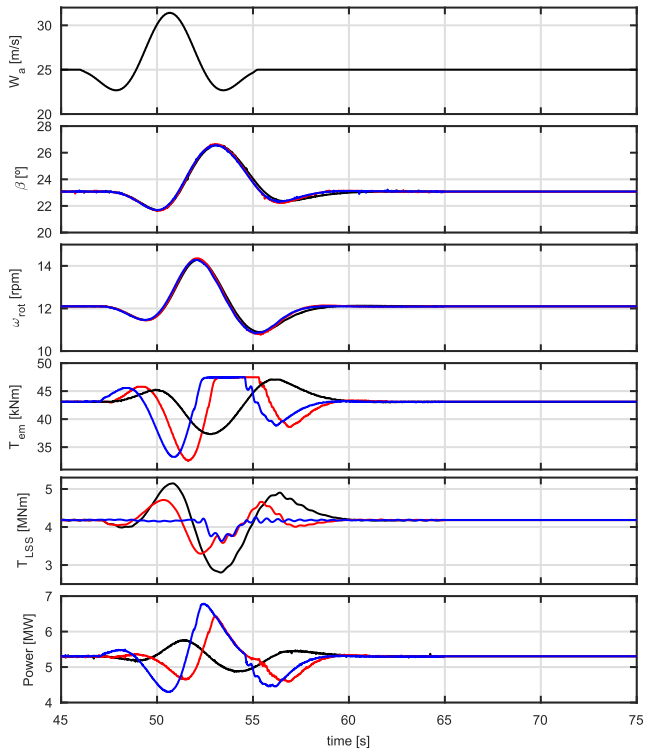

FIGURE 3. Experimental performance on extreme gust at v_{out} = 25 m/s: Baseline control (black), SMPC versions MDL (blue) and UD (red).

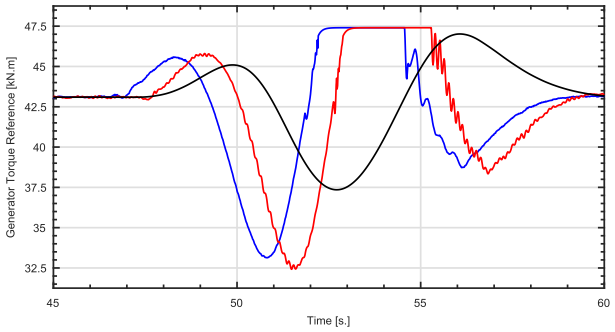

FIGURE 4. Manipulated variables T^*_{em} on extreme gust at v_{out} = 25 m/s. Baseline control (black), SMPC versions MDL (blue) and UD (red).

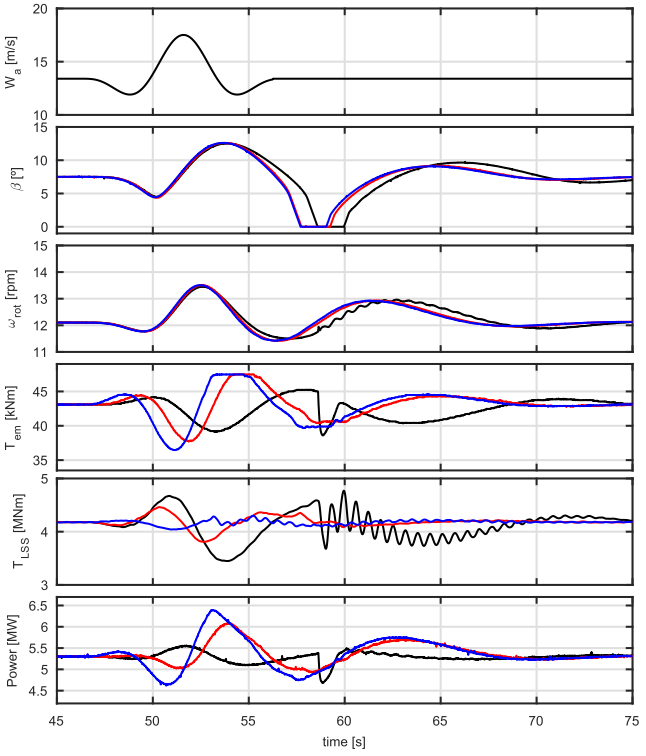

FIGURE 5. Experimental performance on extreme gust at v_{rated}+2 m/s = 13.2 m/s and 10 % internal model error: Baseline control (black), SMPC versions MDL (blue) and UD (red).

improvement is obtained without increasing notably the variation of the generated mechanical power with respect to the UD case.

Next, to study the robustness to model parameter uncertainly, as in section III. A, an increment in the rotor inertia, producing a 10% error in the torsional frequencies of the internal model of the SMPCs, is introduced. Again, the same signals of interest, obtained by the two SMPC versions and the baseline controller under extreme down (v_{rated}+2m/s = 13.2 m/s) operation gust, according to IEC standard, are depicted in Fig. 5. Besides, *Table* 1 presents the experimental load reduction (in %) with respect to the baseline, numerically.

The obtained reduction on the extreme loads on the torsional torque on the *low-speed* shaft (T_{LSS}) -and the corresponding vibrations on the transmission train-, thanks to the LIDAR disturbance previsualization, are again apparent on Fig. 5 and, numerically, in *Table* 1, even with an important error in the model. Thus, the SMPC-MDL robustness to model parameter uncertainly is demonstrated.

On the other hand, *Table* 1 shows that the significant drop in performance suffered by the UD version of the SMPC when relaxing the settings of the controller and state estimator with respect to the simulation-based study -see [23] for more details-, does not take place in the LIDAR-assisted version (MDL). It is probably due to the effect of the anticipation of the control action that allows maintaining the performance despite using a less aggressive setting.

2) FATIGUE LOADS

The responses to the 15 % turbulent wind of mean speed of 24 m/s, when a 10 % error is present in the internal model of the SMPC versions, are now displayed in Fig. 6. In addition, *Table 2* presents the obtained improvements in a comparative numerical way. The experimental platform needs 30 seconds to reach Region 3 and, at the second 39, the SMPC controllers are activated to reduce the load.

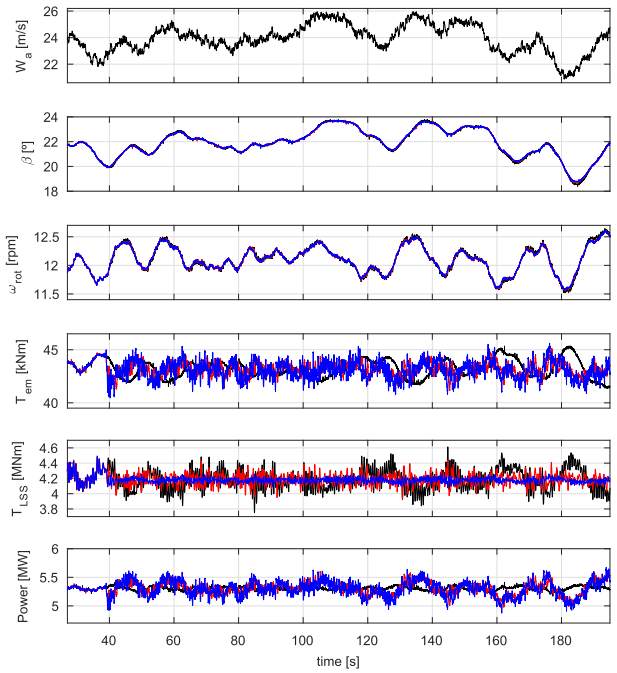

FIGURE 6. Experimental performance on turbulent wind at 24 m/s with 15 % of turbulence and 10 % internal model error: Baseline control (black), SMPC versions MDL (blue) and UD (red).

Again, the obtained improvement by the SMPC-MDL version, based on the perfect previsualization of the incoming effective wind on the rotor, is very high, doubling the drive-train load reduction gained by the UD version. The robustness to model errors seems to be also very high.

IV. REALISTIC LIDAR MEASUREMENTS

A. BACKGROUND

Early work on LIDAR-assisted control [5], [7], [28] assumed that incoming winds could be measured exactly. Thus, it is supposed to be no difference between the measured and actual effective winds and there is no error in the calculation of the instant that such wind reached the rotor. Later, realistic LIDAR models started to be used [7], [29]. Such models included the spatial averaging of the measurements and the limitation of the line-of-sight. In addition, the wind evolution is also included as a source of error in other works [13], [14], [16], taking into account how the wind changes from the time it is measured until it impacts the rotor. Some papers [12], [30] also consider the uncertainty in the calculation of the instant in which the wind actually reaches the rotor.

It is clear that implementing a feedforward-based control, when the preview signal includes too much error, implies some risk, since the controller reacts to such error, turning its action into something potentially counterproductive. Therefore, many recent works, focused on the design of LIDAR-assisted controllers [9], [31], propose characterizing the measurement error and filtering the signal to eliminate the components that do not maintain sufficient correlation with the effective wind, actually reaching the rotor. Besides, others [11], [33] propose to include such correlation directly in an optimal control scheme.

On the other hand, it has been shown [32], [34] that, by soundly manipulating the preview obtained from the LIDAR measurements, it is possible to notably improve the estimate that can be made of the disturbance that the incoming wind will actually cause in the rotor. Specifically, in *Simley et al.* [32] –see also [21] and [36]-, a minimum mean square error (MMSE) estimate of the effective approaching wind can be obtained by using an optimal filter whose design depends on the mentioned correlation between the LIDAR measurement and the actual disturbance. To calculate such correlation, the true wind disturbance must be estimated [35], by roughly using the turbine as an anemometer. In these works, the mentioned filtering should cover the control actuator bandwidth, that, is, up to 1 Hz. Very recently, an artificial neural network (ANN) trained online is used in [37] to soundly correct the errors of the LIDAR previsualization.

B. REALISTIC LIDAR MEASUREMENTS GENERATION

For wind speeds above nominal, the WT control goals are focused on regulating the rotor speed and minimizing the structural load, while keeping the control action limited. Achieving such goals allows the turbine lifetime to be notably increased and, therefore, the cost of energy to be reduced. The benefit of using a LIDAR sensor in order to achieve such control objectives depends on the measurement coherence, that is, the correlation as a function of frequency between the anticipated wind measurement and the one that the turbine will actually receive.

Our aim now is to use a method, well established in the literature, to generate realistic LIDAR measurements with different quality levels. Then, such measurements are used in the real-time control experiments in order to determine the impact of the LIDAR measurement quality on the SMPC control performance. The main finding will be to determine how good these previews must be for the performance to be good enough in order to justify the use of a LIDAR sensor.

One way to define formally such measurement coherence as a function of frequency (f) is given by

$$\gamma_{am}^2(f) = \frac{|S_{am}(f)|^2}{S_{aa}(f)\,S_{mm}(f)} \tag{2}$$

where $\gamma_{am}^2(f)$ it is the magnitude squared coherence, $S_{am}(f)$ is the cross power spectral density between the *measured* wind W_m and the *actual* wind W_a experienced by the turbine. Such wind W_a is estimated by an observer using the turbine itself as an anemometer [35]. Normally, such a method provides a good estimate up to frequencies covering the bandwidth of interest. On the other hand, $S_{mm}(f)$ and $S_{aa}(f)$ are the individual power spectral densities of the measured and actual signal, respectively.

Such squared coherence magnitude can go from one to zero, where one indicates perfect correlation. Therefore, a correlation of less than one means that the measurement includes errors that, in this case, maybe due to measurement noise, wind evolution occurred from focal length, and WT induction zone. The mentioned last two errors are more important at high frequencies, causing the coherence to go normally from values close to one at low frequencies to values close to zero at high frequencies. The exact shape of the coherence function depends on the configuration of the LIDAR sensor and wind and environmental conditions. Evidently, such function shape may be also altered if some advanced method, like those described in [32], [37], is applied to the sensor output to improve the coherence of the signal.

In order to study the influence that the quality of the T_{aero} preview, extracted from in advance incoming wind measurements, has on the performance of the LIDAR-assisted SMPC, the method, proposed in *Dunne and Pao* [33], to generate realistic LIDAR measurements with different coherence profiles, will be here followed. In such motivating work, the actual wind W_a is generated and, after the preview delay, applied to the WT aerodynamic model. Meanwhile, the wind measured by the LIDAR W_m, which is then sent to become an input to our SMPC MDL controller –see Figures 1 and 2-, is calculated according to

$$W_m = LW_a + Hn \tag{3}$$

where L is a low-pass filter, H is a high-pass filter and n is white noise. Filters L and H are designed to achieve that the coherence shape, as a function of the frequency, between W_m and W_a, is the desired one and that the power spectrums of both signals match, that is, $S_{aa} = S_{mm}$. It is convenient that $S_{aa} = S_{mm}$ because the difference in power spectrums could affect the controller gain. So, we have –see [33]-

$$|L| = \sqrt{coh(f)} \tag{4}$$

$$\angle L = 0 \tag{5}$$

$$|H| = \sqrt{|W_a|^2\left(1 - |L|^2\right)} \quad \wedge \quad \angle H = irrelevant \tag{6}$$

where *coh(f)* is the coherence of the LIDAR-based measurement, defined as in the expression (2), that we wish to obtain between W_m and W_a. The magnitudes for the H and L filters obtained by expressions (4) and (6) ensure that the coherence shape is *coh(f)* and that $S_{aa} = S_{mm}$. The phase for filter L in expression (5) ensures that the average phase between W_m and W_a is zero, which is the case when we have correctly calculated and imposed the preview time.

As in [33], a *Butterworth* low-pass filter of order 1 is used for L. Then, several coherence target functions, for different bandwidths (cutoff frequencies, where the magnitude of the filter response is $(0.5)^{1/2}$ of its DC value) of interest for our filter L are obtained. Using such coherence functions, digital filter L is calculated by applying expression (4). However, it is impossible to obtain a causal filter that also meets the condition (5). To roughly solve this problem, the phase of L is approximately converted first to a time delay, extracted by using a very low frequency of the bandwidth. Then, such delay is added to the preview delay applied to W_a before it feeds the aerodynamic model –see figure 2-. In this way, although it is not really fulfilled expression (5), the preview time imposed between W_m and W_a is approximately correct. Finally, expression (6) may be used to design the H filter.

C. APPROACH AND BANDWIDTH RANGE

This study on the impact of the LIDAR coherence does not apply to extreme loads, since the prediction of gusts is hardly affected by the considered measurement errors, given the spectral content of such gusts. Therefore, only the reduction of fatigue load caused by turbulent wind in the transmission train is considered here. More precisely, the aim of our approach relies on how the performance of the LIDAR-assisted SMPC control is affected by the preview errors, within a plausible range, for turbulent winds in region 3.

Since the present approach needs a scenario as realistic as possible, the control experiments have been exclusively performed on the NREL 5MW WT HiL Simulator. Such WT HiL simulator has been described in section III. B. and used to obtain the experimental results presented in section III. C., for the ideal LIDAR case. Besides, the SMPC controller and state observer settings are the same as those used in section III.C and the version MD without preview [23]. However, the design of the LIDAR block in the WT HiL simulator -see Figure 2-, that was transparent ($W_m = W_a$) then, has now been altered. For the present study, such block implements the operation described in section IV. B and defined by expressions (3)-(6), according to the scheme shown in Fig. 7.

On the other hand, using the LIDAR patterns studied by *Schlipf* [38] for the NREL 5MW WT, the coherence bandwidth (BW) range can reach 0.2186 Hz. in the best case, for

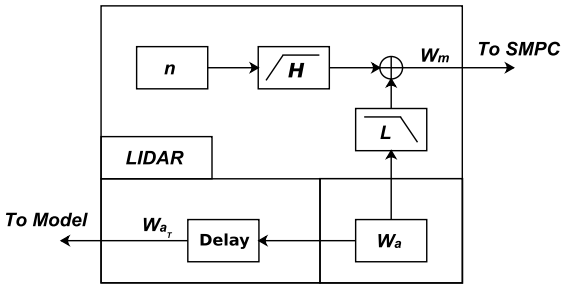

FIGURE 7. LIDAR block in NREL 5MW WT HIL Simulator: Experimental generation of realistic LIDAR measurements.

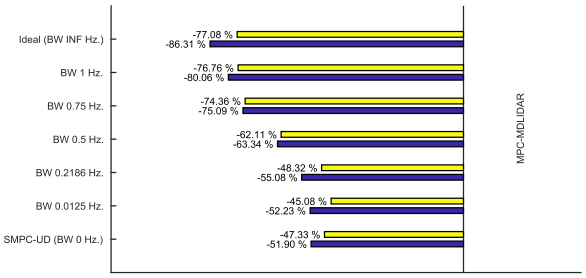

FIGURE 8. Experimental load reduction of the SMPC-MDL for different LIDAR coherence bandwidths on turbulent wind at 14 m/s with 18 % of turbulence: No model error (blue) and 10 % model error (yellow).

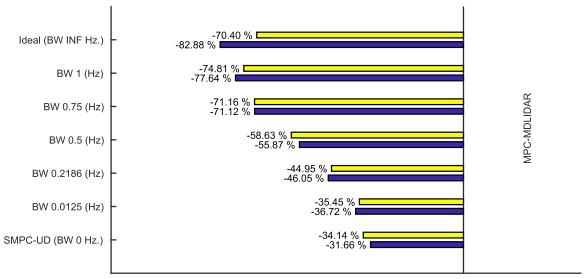

FIGURE 9. Experimental load reduction of the SMPC-MDL for different LIDAR coherence bandwidths on turbulent wind at 18 m/s with 17 % of turbulence: No model error (blue) and 10 % model error (yellow).

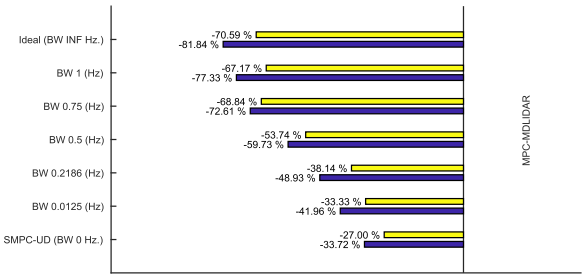

FIGURE 10. Experimental load reduction of the SMPC-MDL for different LIDAR coherence bandwidths on turbulent wind at 24 m/s with 15 % of turbulence: No model error (blue) and 10 % model error (yellow).

the LIDAR configuration used there -see also [33]-. However, given the mentioned works of *Simley et al.* [32], [35], [36], in this study the bandwidth of interest has been extended up to 1 Hz, that is, the bandwidth of the pitch actuator, as it is where their method based on optimal filters may provide sufficient coherence. In our case, the preliminary idea is that the generator torque SMPC control system under study here could take advantage of a preexistent LIDAR preview taken for a pitch feedforward control system -for example, those described in [9], [33], [36] that may be working in parallel. Of course, the settings of a LIDAR sensor may be reconfigured in order to optimize the *in advance* wind measurements for its use with the load reduction SMPC controller. Besides, it is probable that, in such a case, a broader bandwidth for the wind previsualization could be obtained.

V. REALISTIC PERFORMANCE FOR THE LIDAR-ASSISTED SMPC (REAL-TIME CONTROL EXPERIMENTS RESULTS)

A. EXTREME LOADS

As stated before –see section IV. C-, the experimental real-time control results remain approximately the same for realistic previews of the incoming wind –see section III.C.1-.

B. FATIGUE LOADS

The HiL Simulator for the NREL 5 MW WT has been fed with turbulent winds, generated again with *Turbsim* [26], of 14, 18 and 24 m/s. of average speed and turbulences of 18 %, 17 % and 15 %, respectively. The corresponding realistic LIDAR readings have been generated following the procedure described in section IV. The obtained results for the torsional load of the turbine shaft have been processed to calculate the DELs that describe the fatigue load. Then, the experimental tests have been repeated considering an internal model with an error in the natural vibration frequencies up to 10 %. The results regarding the DEL percentage improvement, with respect to the baseline control, of the LIDAR-assisted SMPC controllers, are presented in Figures 8, 9 and 10, for the three mentioned average wind speeds, respectively. The bandwidth -cutoff frequencies, where the magnitude of the L filter response is $(0.5)^{1/2}$ of its DC value- of the LIDAR previsualization used by the SMPC-MDL is in the Y-axis. Within such bandwidth, the magnitude squared coherence, between the anticipated wind measurement and the one that the turbine is actually experiencing, is supposed to be sufficiently good. The improvements obtained by using an ideal LIDAR (BW INF Hz) and SMPC-UD (say, BW 0Hz) is also incorporated to that axis as limiting references.

Note 3: When the LIDAR previsualization gives no useful information about the stochastic nature of the incoming wind (BW = 0 Hz.), the wind preview W_m may be described as a DC offset (wind average speed) plus white noise. In such a case, given the structure of the SMCP LIDAR-assisted version –see Fig. 1-, the additional input ΔT_{aero}, defined as an unmeasured disturbance (UD1), represents now the whole T_{aero} and the SMPC *Kalman Filter* remains in charge of estimating it. In this way, the SMPC MDL version "*converges*" to the UD version, when the LIDAR measurements coherence is completely lost.

Therefore, it may be seen in Figures 8-10 how the quality of the wind preview affects the comparative performance of the LIDAR-assisted SMPC-MDL version, related to the performance achieved by the UD version -without preview-. By considering preview coherence bandwidths between 1 and 0.0125 Hz, it is clear that the obtained load reduction monotonically decreases, as the preview coherence decreases, from the ideal LIDAR (perfect preview) to the SMPC-UD (no preview) case. The robustness to model parameter uncertainly behaves in a very similar fashion.

Anyway, it turns out to be crucial to obtain sufficiently reliable LIDAR measurements of the incoming wind to justify the use of the preview-assisted SMPC option. In particular, for this case study, it seems mandatory to apply some technique in order to improve the quality of the preview for high frequencies (up to 0.75 Hz.-1 Hz.), as those described in [21], [32], [36] and, very recently, [37]. Only by obtaining sufficient coherence in such bandwidths, the obtained reductions in the drive train load are big enough to justify the use of LIDAR.

Finally, the responses to the 15 % turbulent wind of mean speed of 24 m/s, when a 10 % error in the internal model of the SMPC versions is present, and a LIDAR preview with 1 Hz. coherence bandwidth is used, are now displayed in Fig. 11. Again, the experimental platform needs 30 seconds to reach Region 3, and, at second 39, the SMPC controllers are activated to reduce the load. Right then, it may be seen how, indeed, the torque on the shaft T_{LSS} is remarkably stabilized with respect to the baseline case and the SMPC UD version. The vibrations associated with natural frequencies related to the flexibility of the main mechanical components of the turbine are also largely eliminated from the pitch angle β and rotor speed ω_{rot}. On the other hand, the generator torque T_{em} activity is significantly increased compared to the baseline control and this, in turn, is partly transferred to the generated mechanical power $T_{em}\omega_{gen}$.

However, as we may observe, by comparing Fig. 6 and 11 –and also in Fig. 10-, the load reduction when a LIDAR preview coherence bandwidth of 1 Hz., is only slightly impaired with respect to the perfect preview case (70,59 to 67,17 % load reduction). Even more, the control effort in T_{em} and the corresponding disturbance in the generated mechanical power has been reduced.

To verify this effect, Figure 12 shows the electric power measured by the REGEN Unidrive unit in the NREL WT 5MW HiL Simulator hardware –scaled-. As we can see, the power provided to the grid, when a realistic LIDAR preview is used, seems less disturbed than when using a "perfect" preview or even the SMPC UD version, without wind previsualization. Therefore, if an effective wind preview, with sufficient coherence up to about 1 Hz, is achieved, the use of LIDAR-assisted SMPC control is fully justified.

At this point, in order to further confirm such important assertion, it seems appropriate to complete the study with a frequency analysis of the signals of interest presented in Figures 11 and 12. Therefore, the *Fast Fourier Transforms*

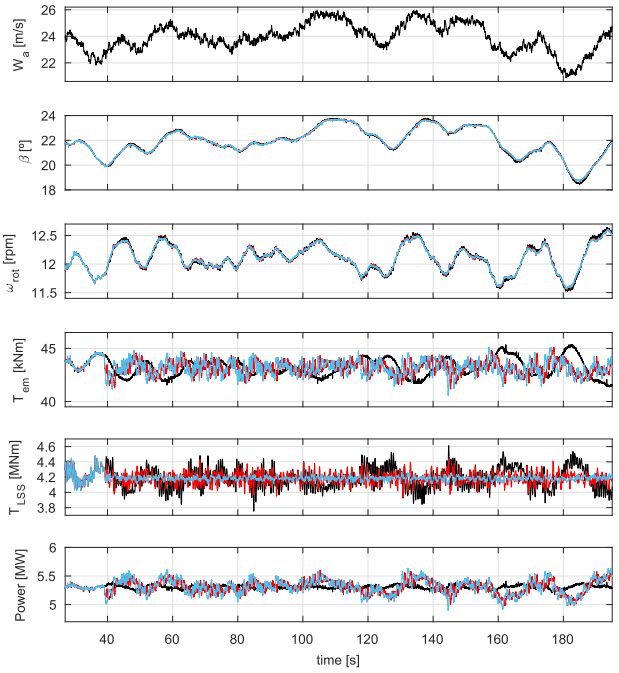

FIGURE 11. Experimental performance on turbulent wind at 24 m/s with 15 % of turbulence and 10 % internal model error: Baseline control (black) and SMPC versions MDL with 1 Hz. LIDAR coherences bandwidth (light blue) and UD (red).

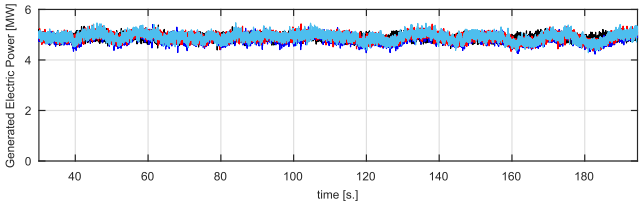

FIGURE 12. Generated electrical power measured –scaled- by the REGEN Unidrive unit in the NREL 5MW turbine HIL Simulator. Turbulent wind at 24 m/s with 15 % of turbulence and 10 % internal model error: Baseline control (black) and SMPC versions: MDL (blue), UD (red) and MDL with 1 Hz. LIDAR measurement bandwidth (light blue).

(FFT) of such signals have been calculated and presented in Figure 13. In such a figure, it may be seen that the effects of the torsional vibrations on pitch angle, generator speed, and low-speed shaft torque are greatly attenuated. It may also be seen that the power of some frequency components is increased to some extent in the generator torque and, correspondingly, in the generated mechanical power. However, we may also see that the frequency components of the generated electrical power, supplied to the grid by the three controllers on the comparison, are very similar.

Note 4: Let's look one more time, in figure 13, at the generated power FFTs, both mechanical and electrical. It may be seen that *only* the very low-frequency components (below 0.75 Hz., approximately) of the increase in the disturbances, observed in the mechanical power -due to the control action-, pass clearly through the DC bus to reach the electrical power, supplied to the grid. This effect can also be seen in

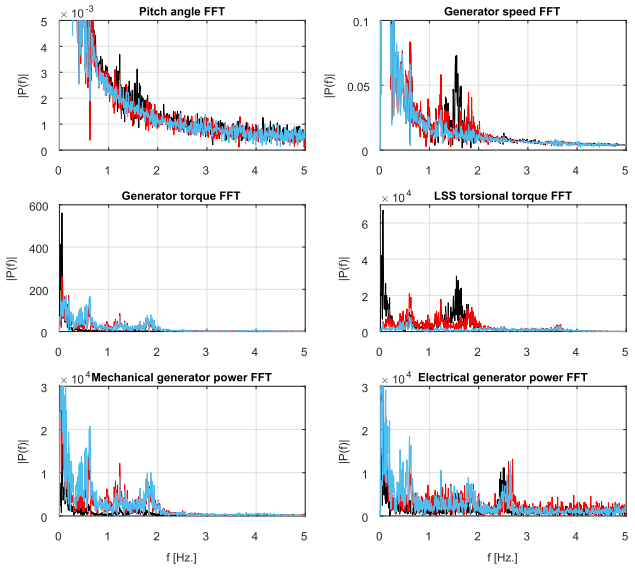

FIGURE 13. Fast Fourier Transforms of signals of interest in figures 11 and 12. Turbulent wind at 24 m/s with 15 % of turbulence and 10 % internal model error: Baseline control (black) and SMPC versions: UD (red) and MDL with 1 Hz. LIDAR measurement bandwidth (light blue).

figures 11 and 12. Such disturbances, as shown in figure 11, are caused by the low-frequency oscillations in ω_{rot}, due to the performance of the pitch control loop, which are then transferred to ω_{gen} and, finally, to the generated power. Fortunately, these observed fluctuations in the electrical power are relatively small in magnitude –see figure 12-. However, if necessary, they could be avoided when applying the SMPC controllers, by renouncing -partially or totally- to prevent their impact on the torsion of the shaft. In order to do this, we should inject such low-frequency fluctuation -in counter phase- into the SMPC low-speed shaft torque reference T^*_{LSS}, via ω_{genf} (remember, $T^*_{LSS} = P_{rated}/\omega_{rot} = P_{rated}N_{gear}/\omega_{genf}$). By now, ω_{genf} is fixed at the ω_{gen} nominal value, given that the present study aims to analyze the SMPC capacity to *reduce at a minimum* the WT structural load. Now, alternatively, to obtain ω_{genf}, we may low-pass filter ω_{gen} measurement by using *cut-off* frequencies around 1 Hz. -see FFTs of the generator powers in figure 13- and add the result in counterphase to the ω_{gen} nominal value. In this way, it would be possible to importantly reduce the fatigue load on the transmission train originated by the elasticity of the shaft and rotor (1.7 and 4 Hz.), while allowing –partially or totally, at will- the low-frequency shaft torsion in order not to convert such mechanical vibrations into electrical ones. By designing the low-pass filter -cutoff frequency and order- used to produce ω_{genf}, we may balance the partial transmission of mechanical vibrations to electrical disturbances in the context of the wind turbine controller.

C. COMPUTATIONAL BURDEN

The real-time controllers have been implemented on an Intel Core2 Duo E8400 3 GHz industrial computer equipped with *Simulink Real-Time* –see [39]- kernel. The KWIK algorithm –see [40]- has been used to solve the optimization quadratic problem. The SMPC controllers have been implemented by using a standard 80 Hz. sampling frequency. The maximum computational delays for de LIDAR-assisted version was 5,129e-5 s., corresponding to a maximum number for iterations of 7. On the other hand, the more compact UD version has given a maximum computational delay of 3,41e-5 s. with 4 iterations at most. In both cases, the computational burden does not reach 0.4 % and, therefore, the corresponding delay is negligible. Further details are available in [23].

VI. CONCLUSION

In this paper, a single model-based predictive controller taking advantage of the incoming wind in advance measurements is applied to the torque of a wind turbine generator in order to reduce structural loads. First, to analyze the potential performance of such a controller, it is assumed that the effective wind preview is perfect. In this way, very important reductions are obtained with respect to the case without preview, for both extreme loads and fatigue, during the experimental real-time control tests that are carried out on rapid controller prototypes working versus a reference wind turbine Hardware-in-the-Loop simulator. However, it is also demonstrated later that these improvements are conditioned to have an effective wind preview presenting an acceptable coherence with respect to the actual wind, for a sufficiently wide bandwidth. In fact, for this case study, it may be necessary the use an advanced method (optimal filters, neural networks, ...) to improve this preview or, alternatively, the custom configuration of the used *LIght Detection And Ranging* (LIDAR) sensor for this controller. Incorporating more wind turbine sensor measurements into the described approach and studying the effect on the obtained performance remains as future work.

REFERENCES

[1] N. Kodama, T. Matsuzaka, K. Tuchiya, and S. Arinaga, "Power variation control of a wind generator by using feed-forward control," *Renew. Energy*, vol. 16, n. 1-4, pp. 847–850, Jan-Apr. 1999, doi: 10.1016/S0960-1481(98)00283-3.

[2] M. Harris, M. Hand, and A. Wright, "LIDAR for turbine control," Nat. Renew. Energy Lab., Golden, CO, USA, Tech. Rep. NREL/TP-500-39154, Jan. 2006.

[3] E. A. Bossanyi, A. Kumar, and O. Hugues-Salas, "Wind turbine control applications of turbine-mounted LIDAR," *J. Phys., Conf. Ser.*, vol. 555, Dec. 2014, Art. no. 012011, doi: 10.1088/1742-6596/555/1/012011.

[4] D. Schlipf, P. Fleming, S. Kapp, A. Scholbrock, F. Haizmann, F. Belen, A. Wright, and P. Wen Cheng, "Direct speed control using LIDAR and turbine data," in *Proc. Amer. Control Conf.*, Jun. 2013, pp. 2208–2213, doi: 10.1109/ACC.2013.6580163.

[5] D. Schlipf and M. Kühn, "Prospects of a collective pitch control by means of predictive disturbance compensation assisted by wind speed measurements," in *Proc. German Wind Energy Conf. (DEWEK)*, Bremen, Germany, Nov. 2008, pp. 1–4, doi: 10.18419/opus-3900.

[6] D. Schlipf, T. Fischer, C. E. Carcangiu, M. Rossetti, and E. Bossanyi, "Load analysis of look-ahead collective pitch control using LIDAR," in *Proc. German Wind Energy Conf. (DEWEK)*, Bremen, Germany, Nov. 2010, doi: 10.18419/opus-3902.

[7] F. Dunne, L. Pao, A. Wright, B. Jonkman, N. Kelley, and E. Simley, "Adding feedforward blade pitch control for load mitigation in wind turbines: Non-causal series expansion, preview control, and optimized FIR filter methods," in *Proc. 49th AIAA Aerosp. Sci. Meeting Including New Horizons Forum Aerosp. Expo.*, Jan. 2011, p. 819, doi: 10.2514/6.2011-819.

[8] N. Wang, K. E. Johnson, and A. D. Wright, "FX-RLS-Based feedforward control for LIDAR-enabled wind turbine load mitigation," *IEEE Trans. Control Syst. Technol.*, vol. 20, no. 5, pp. 1212–1222, Sep. 2012, doi: 10.1109/TCST.2011.2163515.

[9] D. Schlipf, L. Y. Pao, and P. W. Cheng, "Comparison of feedforward and model predictive control of wind turbines using LIDAR," in *Proc. IEEE 51st IEEE Conf. Decis. Control (CDC)*, Dec. 2012, pp. 3050–3055, doi: 10.1109/CDC.2012.6426063.

[10] D. Schlipf, D. J. Schlipf, and M. Kühn, "Nonlinear model predictive control of wind turbines using LIDAR," *Wind Energy*, vol. 16, no. 7, pp. 1107–1129, Oct. 2013, doi: 10.1002/we.1533.

[11] F. Dunne and L. Y. Pao, "Benefit of wind turbine preview control as a function of measurement coherence and preview time," in *Proc. Amer. Control Conf.*, Jun. 2013, pp. 647–652, doi: 10.1109/ACC.2013.6579910.

[12] M. Mirzaei, M. Soltani, N. K. Poulsen, and H. H. Niemann, "Model predictive control of wind turbines using uncertain LIDAR measurements," in *Proc. Amer. Control Conf. (ACC)*, Washington, DC, USA, Jun. 2013, pp. 2235–2240, doi: 10.1109/ACC.2013.6580167.

[13] M. Kristalny, D. Madjidian, and T. Knudsen, "On using wind speed preview to reduce wind turbine tower oscillations," *IEEE Trans. Control Syst. Technol.*, vol. 21, no. 4, pp. 1191–1198, Jul. 2013, doi: 10.1109/TCST.2013.2261070.

[14] C. L. Bottasso, P. Pizzinelli, C. E. D. Riboldi, and L. Tasca, "LiDAR-enabled model predictive control of wind turbines with real-time capabilities," *Renew. Energy*, vol. 71, pp. 442–452, Nov. 2014, doi: 10.1016/j.renene.2014.05.041.

[15] J. Laks, L. Pao, E. Simley, A. Wright, N. Kelley, and B. Jonkman, "Model predictive control using preview measurements from LIDAR," in *Proc. 49th AIAA Aerosp. Sci. Meeting Including New Horizons Forum Aerosp. Expo.*, Jan. 2011, p. 813, doi: 10.2514/6.2011-813.

[16] J. Laks, E. Simley, and L. Pao, "A spectral model for evaluating the effect of wind evolution on wind turbine preview control," in *Proc. Amer. Control Conf.*, Jun. 2013, pp. 3673–3679, doi: 10.1109/ACC.2013.6580400.

[17] K. A. Kragh, M. H. Hansen, and L. C. Henriksen, "Sensor comparison study for load alleviating wind turbine pitch control," *Wind Energy*, vol. 17, no. 12, pp. 1891–1904, Dec. 2014, doi: 10.1002/we.1675.

[18] K. A. Kragh, M. H. Hansen, and T. Mikkelsen, "Precision and shortcomings of yaw error estimation using spinner-based light detection and ranging," *Wind Energy*, vol. 16, no. 3, pp. 353–366, Apr. 2013, doi: 10.1002/we.1492.

[19] D. Schlipf, S. Kapp, J. Anger, O. Bischoff, M. Hofsäß, A. Rettenmeier, U. Smolka, and M. Kühn, "Prospects of optimization of energy production by LIDAR assisted control of wind turbines," in *Proc. Eur. Wind Energy Assoc. (EWEA) Annu. Event*, Brussels, Belgium, Mar. 2011, pp. 1–7, doi: 10.18419/opus-3916.

[20] A. Scholbrock, P. Fleming, D. Schlipf, A. Wright, K. Johnson, and N. Wang, "Lidar-enhanced wind turbine control: Past, present, and future," in *Proc. Amer. Control Conf. (ACC)*, Jul. 2016, pp. 1399–1406, doi: 10.1109/ACC.2016.7525113.

[21] E. Simley, H. Fürst, F. Haizmann, and D. Schlipf, "Optimizing lidars for wind turbine control applications—Results from the IEA wind task 32 workshop," *Remote Sens.*, vol. 10, no. 6, p. 863, Jun. 2018, doi: 10.3390/rs10060863.

[22] A. Clifton, P. Clive, J. Gottschall, D. Schlipf, E. Simley, L. Simmons, D. Stein, D. Trabucchi, N. Vasiljevic, and I. Würth, "IEA wind task 32: Wind lidar identifying and mitigating barriers to the adoption of wind lidar," *Remote Sens.*, vol. 10, no. 3, p. 406, Mar. 2018, doi: 10.3390/rs10030406.

[23] R. Barcena, T. Acosta, A. Etxebarria, and I. Kortabarria, "Wind turbine structural load reduction by linear single model predictive control," *IEEE Access*, vol. 8, pp. 98395–98409, 2020, doi: 10.1109/ACCESS.2020.2996381.

[24] M. L. Buhl, "WT_Perf user's guide," NREL, Nat. Renew. Energy Lab., Golden, CO, USA, Tech. Rep. NREL/TP-500-41136, 2004.

[25] *Wind Turbines_Part I: Design Requirements*, 3rd ed, document IEC 61400-1, 2005.

[26] B. J. Jonkman and M. L. Buhl, "TurbSim user's guide," Nat. Renew. Energy Lab., Golden, CO, USA, Tech. Rep. NREL/TP-500-41136, Apr. 2007.

[27] E. Bossanyi, B. Savini, M. Iribas, M. Hau, B. Fischer, D. Schlipf, T. Engelen, M. Rossetti, and C. E. Carcangiu, "Advanced controller research for multi-MW wind turbines in the UPWIND project," *Wind Energy*, vol. 15, no. 1, pp. 119–145, Jan. 2012, doi: 10.1002/we.523.

[28] J. Laks, L. Pao, A. Wright, N. Kelley, and B. Jonkman, "The use of preview wind measurements for blade pitch control," *Mechatronics*, vol. 21, no. 4, pp. 668–681, Jun. 2011, doi: 10.1016/j.mechatronics.2011.02.003.

[29] E. Simley, L. Y. Pao, R. Frehlich, B. Jonkman, and N. Kelley, "Analysis of light detection and ranging wind speed measurements for wind turbine control," *Wind Energy*, vol. 17, no. 3, pp. 413–433, Mar. 2014, doi: 10.1002/we.1584.

[30] F. Dunne, L. Y. Pao, D. Schlipf, and A. K. Scholbrock, "Importance of LIDAR measurement timing accuracy for wind turbine control," in *Proc. Amer. Control Conf. (ACC)*, Portland, OR, USA, Jun. 2014, pp. 3716–3721, doi: 10.1109/ACC.2014.6859337.

[31] A. Scholbrock, P. Fleming, L. Fingersh, A. Wright, D. Schlipf, F. Haizmann, and F. Belen, "Field testing LIDAR-based feed-forward controls on the NREL controls advanced research turbine," in *Proc. 51st AIAA Aerosp. Sci. Meeting Including New Horizons Forum Aerosp. Expo.*, Jan. 2013, p. 818, doi: 10.2514/6.2013-818.

[32] E. Simley and L. Pao, "Reducing LIDAR wind speed measurement error with optimal filtering," in *Proc. Amer. Control Conf.*, Jun. 2013, pp. 621–627, doi: 10.1109/ACC.2013.6579906.

[33] F. Dunne and L. Y. Pao, "Optimal blade pitch control with realistic preview wind measurements," *Wind Energy*, vol. 19, no. 12, pp. 2153–2169, Dec. 2016, doi: 10.1002/we.1973.

[34] D. Schlipf, P. Fleming, F. Haizmann, A. Scholbrock, M. Hofsäß, A. Wright, and P. W. Cheng, "Field testing of feedforward collective pitch control on the CART2 using a nacelle-based lidar scanner," *J. Phys., Conf. Ser.*, vol. 555, Dec. 2014, Art. no. 012090, doi: 10.1088/1742-6596/555/1/012090.

[35] E. Simley and L. Y. Pao, "Evaluation of a wind speed estimator for effective hub-height and shear components," *Wind Energy*, vol. 19, no. 1, pp. 167–184, Dec. 2014, doi: 10.1002/we.1817.

[36] E. Simley, "Wind speed preview measurement and estimation for feedforward control of wind turbines," Ph. D. dissertation, Dept., Elect. Eng., Univ. Colorado at Boulder, Boulder, CO, USA, 2015.

[37] A. R. Araghi, G. H. Riahy, O. Carlson, and S. Gros, "Enhancing the net energy of wind turbine using wind prediction and economic NMPC with high-accuracy nonlinear WT models," *Renew. Energy*, vol. 151, pp. 750–763, May 2020, doi: 10.1016/j.renene.2019.11.070.

[38] D. Schlipf, "LIDAR-assisted control concepts for wind turbines," Ph.D. dissertation, Dept. Inst. Aircr. Des., Universität Stuttgart, Stuttgart, Germany, Jun. 2015, doi: 10.18419/opus-8796.

[39] *Simulink Real-Time User's Guide*, MathWorks, Natick, MA, USA, 2020.

[40] C. Schmid and L. T. Biegler, "Quadratic programming methods for reduced Hessian SQP," *Comput. Chem. Eng.*, vol. 18, no. 9, pp. 817–832, Sep. 1994, doi: 10.1016/0098-1354(94)E0001-4.

RAFAEL BARCENA (Member, IEEE) received the Licenciado and Ph.D. degrees in physics from the University of the Basque Country (UPV/EHU), in 1994 and 2001, respectively. Since 1998, he has been a Researching Professor with the Department of Electronics Technology, UPV/EHU. His research interests include control theory, hybrid control, and sampled-data systems. He has also been an IEEE member (Control Systems and Industrial Electronics Societies), since 2005.

TATIANA ACOSTA received the B.Sc. degree in electronics in automation and control engineering from the Universidad de las Fuerzas Armadas—ESPE, Ecuador, in 2002, and the M.Sc. degree in advanced electronic systems from the University of the Basque Country (UPV/EHU), Spain, in 2016, where she is currently pursuing the Ph.D. degree in electronics and telecommunications. In 2002, she joined the Universidad de las Fuerzas Armadas—ESPE as a Researcher and a Professor. She was a Researcher with the Centro de Investigaciones Científicas y Tecnológicas del Ejército (CICTE), from 2002 to 2012, developing research projects of a military nature.

AINHOA ETXEBARRIA received the M.S. and Ph.D. degrees in electronic engineering from the University of the Basque Country (UPV/EHU), Bilbao, Spain, in 1994 and 2004, respectively. Since 1997, she has been a Researching Professor with the Department of Electronics Technology, UPV/EHU. Her research interests include system identification and computer-controlled systems.

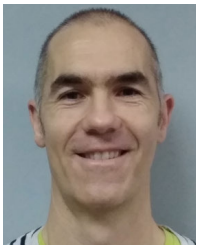

INIGO KORTABARRIA (Member, IEEE) received the M.Sc. degree from the University of Mondragon, Mondragon, Spain, in 1999, and the Ph.D. degree from the University of the Basque Country (UPV/EHU), Bilbao, Spain, in 2013, all in electronics and control engineering. From 1999 to 2004, he was a Research and Development Staff Member in industrial electronics companies. From 2004 to 2014, he was an Assistant Professor of electronic technology with the Department of Electronics Technology, UPV/EHU, where he became an Associate Professor, in 2014. His current research interest includes control of power converter topologies for electric vehicles.